Article:

Jiang, W., He, C., Huang, Y. orcid.org/0000-0002-1220-6896 et al. (4 more authors) (2025) Diffusion of re-suspended dust induced by vehicles: Full-scale simulation and field test. Transportation Research Part D Transport and Environment, 139. 104552. ISSN 1361-9209

https://doi.org/10.1016/j.trd.2024.104552

Diffusion of re-suspended dust induced by vehicles: full-scale simulation and field test

Abstract: Re-suspended road dust refers to the dust settled on road surface that is stirred up again by vehicles, leading to road area air pollution. To better understand the diffusion patterns of these particles, this study simulated the diffusion using high-definition cameras to capture long-persistence luminescent material from a visual media perspective, field measurement using particle counters was carried out to validate the effectiveness. The key findings include: The suction between the tire and ground is crucial for re-suspending particles after rolling. The wake of the vehicle carries particles forward without lateral or vertical diffusion, but negative pressure be-hind the vehicle causes lateral and vertical diffusion. Higher speeds and ground deposit concentrations increase diffusion height and width. To protect pedestrians on overpass and roadside, sidewalks should be placed at a certain distance from road. This study aims to provide data for mitigating road dust re-suspension and aiding computational fluid dynamics simulations.

Keywords: non-exhaust emission; re-suspended dust; long persistence luminescence material; particular matter; road dust

1. Introduction

Non-exhaust emissions refer to particle pollutants generated by vehicles or tire-road contact that are not related to the exhaust from the combustion engine (Roy et al., 2024; Wagner et al., 2024). Brake, tire, and road surface wear are significant contributors to these particulate matters (PM) (Shan et al., 2024). Among them, wear particles such as chromium (Cr), silica (SiO_2), and calcium carbonate ($CaCO_3$) are commonly found within these particulates (Budai and Clement, 2018; Wu et al., 2024a; Wu et al., 2024b; Zou et al., 2023). When these wear particles, along with atmospheric deposition particles, are suspended by vehicle traffic, this phenomenon is referred to as dust of re-suspension or re-suspended dust (Wang et al., 2023; Wang et al., 2024). This significantly affects the concentration of particulate matter 10 (PM_{10}) within the road area and can cause irreversible health damage when inhaled by roadside pedestrians or drivers (Casotti Rienda et al., 2023; Edwards et al., 2022; Li et al., 2024; Roy et al., 2024).

Wang et al. discovered through pavement simulations that vehicle speed and water content significantly affect the PM concentration of road area (Wang et al., 2023). Liu et al. found that resuspended dust contains a significant amount of heavy metals, with Cu primarily originating from traffic emissions (Liu et al., 2023). Jandacka et al. found that the chemical elements Al, Br, Ca, Cl, Cr, Cu were identified in the PM within tunnels (Jandacka et al., 2022). He et al. found that tire wear, asphalt wear, and calcium carbonate are significant sources of traffic-related particles (He and Jiang, 2024; He et al., 2024). Laniyan et al. found that there is a high concentration of heavy metals, especially Pb and Ni, in road pollutants, indicating a deteriorating urban environment

(Laniyan and Popoola, 2024; Yu et al., 2023). Jeong et al. observed that $PM_{2.5}$ emissions were linked to traffic, with brake wear contributing between 16% and 21%. The particles generated by brake wear are nearly equivalent to those produced by road resuspension (Jeong et al., 2019). Svensson et al. found that porous asphalt concrete pavements can reduce dust resuspension by retaining particulate matter within their pores and decreasing the air pumping effect of tires (Svensson et al., 2023).

The rapid urbanization and increasing use of electric vehicles (EVs) and plug-in hybrid electric vehicles (PHEVs) exacerbate the issue of non-exhaust emissions (Jiang et al., 2022). EVs, being heavier than internal combustion engine vehicles (ICEVs), exert greater pressure on components, leading to the generation of more wear particles (Jiang et al., 2022; Timmers and Achten, 2016). These non-exhaust emissions, primarily resulting from vehicle movement and wear rather than fuel combustion, persist regardless of the vehicle's powertrain.(Grange et al., 2021; Guerreiro et al., 2016). Thus, mitigating non-exhaust emissions emerges as a crucial aspect of environmental protection (Abu Khatita, 2024; Laniyan and Popoola, 2024; Wang et al., 2017).

Most researchers focus on the composition, toxicology, and health effects of resuspended dust of non-exhaust emissions (Alves et al., 2020; Samiksha et al., 2017). They typically achieve the above objectives by collecting these particles or conducting point-based measurements using particle counters. However, there has been little research on the suspension mechanisms of these fine particles, largely due to their small size (less than 10 microns). At the same time, studying the suspension mechanisms of these particles can provide strong data support for simulating their diffusion behavior.

Therefore, to fill this significant gap, it is essential to investigate the suspension mechanisms of these particles and conduct visualization studies.

Persistent luminescent materials belong to the category of photoluminescent materials, capable of absorbing and storing external light energy, such as visible or ultraviolet light (Chae et al., 2024; Chen et al., 2016; Dan et al., 2024; Liu et al., 2024; Verma et al., 2020). After the external light source disappears, these materials slowly release the stored energy in the form of light (Jiang et al., 2024; Li et al., 2016; Van den Eeckhout et al., 2013). They can absorb sunlight during the day or artificial light sources and utilize the stored energy in the night or dark environments (Chen et al., 2016). This type of material is also commonly used as tracers to study the compatibility or diffusion behavior of substances. However, such materials have limited luminescent properties, and the fluorescence intensity may not meet the requirements of all applications (Shan et al., 2024; Wu et al., 2024a). In addition, the light scattering involved in the Tyndall effect is a natural optical phenomenon (Huang et al., 2021). It happens when bright light is bent off its straight path due to small uneven areas caused by tiny particles in a gas or liquid. This effect often makes invisible fine particles become visible. The Tyndall effect has many practical uses in everyday life. For example, in colloidal suspensions such as smoke, haze, or milk, we can observe the scattering effect of sunlight passing through them, forming a beam of bright light (Deng et al., 2021). This phenomenon is also used to measure the concentration of suspended particles in liquids or to study the particle content in the atmosphere (Xiao et al., 2019; Yang et al., 2023).

2. Objectives

This study differs from traditional methods by firstly utilizing luminescent materials combined with the Tyndall effect to visually simulate the diffusion patterns of smaller-suspended road particles. By using a car to simulate the diffusion of 10 μm particles, the study offers a visual representation of road dust diffusion patterns and validates these patterns through actual road PM concentration measurements. The objectives of the study are as follows:

1. To establish the relationship between particle diffusion patterns and vehicle-induced conditions, such as speed.
2. To determine the maximum distance of particle diffusion in all directions (X, Y, Z axes) under vehicle flow.
3. To analyze the re-suspension mechanism of particles in traffic-induced flow using visual techniques.

The findings from this experiment can provide valuable data for understanding the re-suspension of traffic-related dust. Additionally, these findings can support Computational Fluid Dynamics (CFD) simulations such particles. It is hoped that this study will contribute positively to efforts aimed at mitigating the health impacts of re-suspended dust, one important contributor of non-exhaust emissions.

3. Materials and methodology

3.1 The overall study method

This study is divided into two parts. The first part, "Long-Persistence Luminescent Material (LPLM) Induced by Vehicle," is a simulation study that investigates the diffusion patterns of re-suspended particles through their capture on camera. The experimental approach involves laying a certain amount of LPLM on the road and subjecting it to rolling by vehicles at various speeds and spreading amount. By processing photos and videos, it can deduce the diffusion patterns of re-suspended particles. The second part, the "Road PM Monitoring" experiment, is designed to verify the results of the first experiment. This involves studying the diffusion width, height, and patterns along the direction of the road of re-suspended dust on actual roads using dust detection instruments. The approach for this experiment includes placing particle counters at various heights and widths or conducting long-term monitoring of a road to validate the diffusion patterns. The overall research method is illustrated in Figure 1.

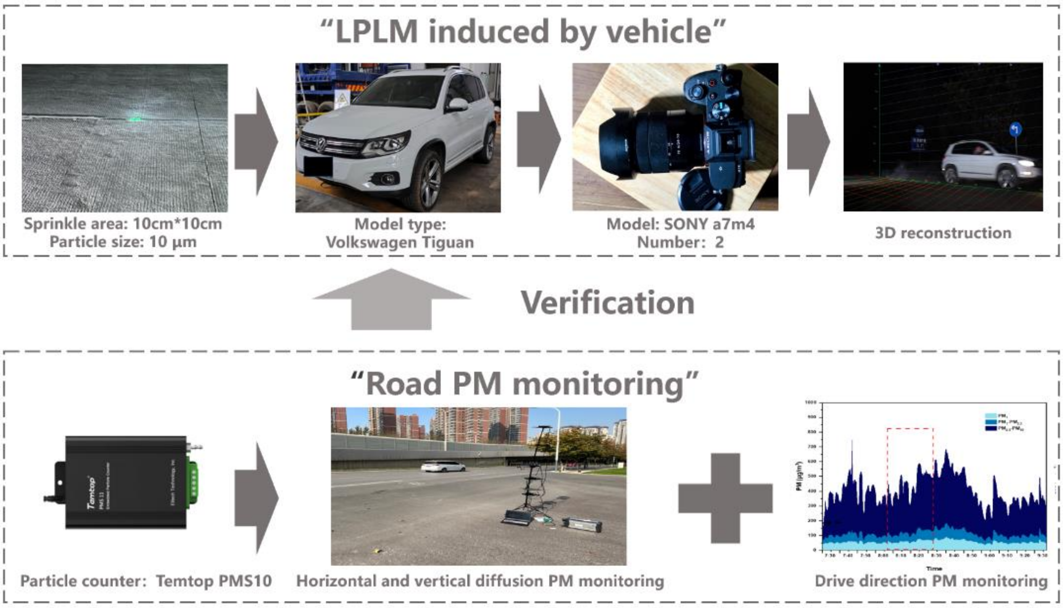

Figure 1. The overall study method

3.2 The experiment method of "LPLM induced by vehicle"

3.2.1 Long persistence luminescence material

The LPLM used in this experiment is manufactured by Guangzhou Zhongming Luminescent Co., Ltd. To capture particles clearly, it is essential that the LPLM has high brightness, making the green material with a longer wavelength more suitable for this purpose. To be compatible with the particle counter, the particle size is uniformly set at 10 μm, as detailed in Table 1. The scattering area on the ground is consistently 10 cm × 10 cm.

Table 1. The index of LPLM

The index of LPLM	Results
Chemical formula	$SrAl_2O_4:Eu^{2+}, Dy^{3+}$
Particle size (μm)	10
Maximum brightness (mcd/m^2)	13091

3.2.2 Camera and shooting position

In the previous pre-experiment, it was observed that relying solely on the luminescent brightness of the long-persistence luminescent material was insufficient for accurate particle capture. This is because, as particles accumulate, their luminescent brightness increases, making observation possible during this period. However, as particles re-suspend, accumulation decreases, making particle diffusion difficult to record with the naked eye or through video capture. Therefore, it is necessary to use a xenon lamp to illuminate the particles, utilizing a principle similar to the Tyndall effect. Ultimately, re-suspended particles not only exhibit their own luminescent brightness but also reflect additional brightness from the illuminated light.

Particle diffusion involves both spatial and temporal dimensions. To accurately determine the diffusion patterns of particles, observations are made from two camera positions. The two positions are angled differently: Camera 1 faces directly along the direction of the roadway, capturing images in both horizontal and vertical directions, while Camera 2 faces laterally to the direction of the road, capturing images in both longitudinal and vertical directions. The images from the two cameras can corroborate each other; for example, the vertical diffusion height in both images at the same moment should be identical. This allows for a reasonable deduction of the horizontal and longitudinal diffusion areas, as shown in Figure 2. The camera used is a Sony A7M4, set to record at 4x slow motion; some parameters are listed in Table 2.

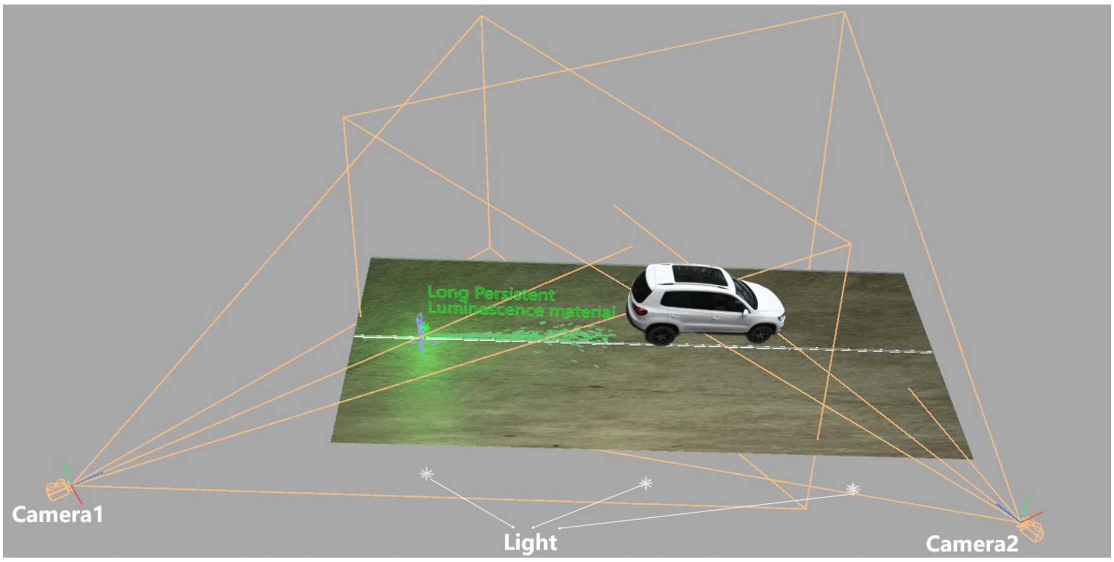

Figure 2. The experiment field of the study

Table 2. The index of the camera

The parameter of camera	Results
Record framerate (p)	25
Frames Per Second (fps)	100
ISO	100
Record speed	0.25×

3.2.3 Test field and vehicle

Prior to the experiment, a day with low wind speed was selected to avoid the influence of atmospheric airflow, and temperature and humidity were recorded. The experimental road is located in a closed test field, and the road surface is cleaned with an industrial vacuum cleaner to eliminate the influence of pre-existing atmospheric settled particles. The vehicle model chosen is the Volkswagen Tiguan. During the experiment, the car completely rolls over the LMLP to simulate real road conditions. The experiment is divided into five speed levels: 20 km/h, 40 km/h, 60 km/h, 80 km/h, and 100 km/h. To investigate the effects of different spreading amounts, experiments are conducted at a constant speed of 60 km/h with spreading amounts of 2 g, 4 g, 6 g, 8 g, 10 g, and 12 g, respectively. The recorded pictures (cut out from the video) are illustrated in Figure 3.

(a)

(b)

Figure 3. Capture the shot from the video: (a) Camera 1 (b) Camera 2

3.2.4 Data processing

3.2.4.1 Residue particles

The residue particles are agglomerated and exhibit a three-dimensional morphology. Thus, image processing is necessary to obtain a three-dimensional distribution. First, the captured photos are cropped to 50 cm, followed by image processing using the Open-Source Computer Vision library (OpenCV) in Python. Due to background interference and other light sources, direct binarization cannot yield satisfactory results. Therefore, the first step involves identifying LMLP particles, followed by Contrast Limited Adaptive Histogram Equalization (CLAHE) for low-light enhancement to maximize particle visibility. The enhanced image is then binarized to observe the two-dimensional distribution on the ground. As the thickness of the accumulated particles on the ground increases, the light intensity becomes stronger. Converting the luminosity to color through pseudo-colorization reveals vertical distribution patterns of residue particles on the ground, as shown in Figure 4.

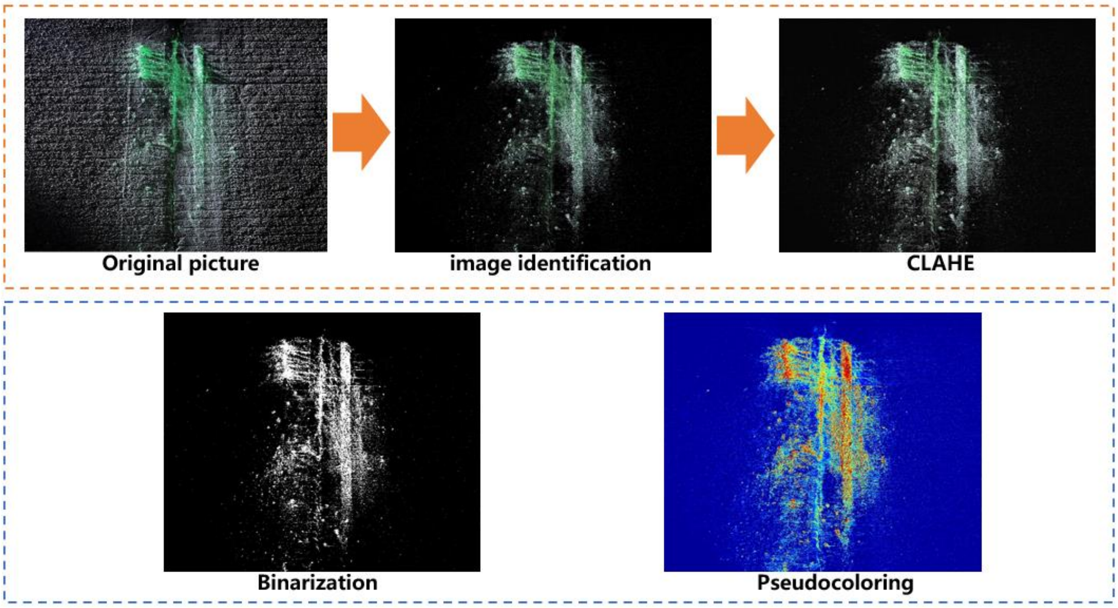

Figure 4. The analysis processes of residue particles

3.2.4.2 Re-suspended particles

Similarly, re-suspended particles in the air also disperse in three-dimensional space. Therefore, to accurately determine their diffusion pattern, it is essential to establish a three-dimensional coordinate system in the video. Prior to this, panoramic marker measurements of the experimental site should be conducted, including markers, street-lights, and the lengths of cement joints on the ground. The three-dimensional coordinate system is then drawn and mapped onto the video, with the result shown in Figure 5 (the figure is a frame captured from the video). Frames containing the three-dimensional coordinate system were extracted from the video, with one image per second. Since the footage was shot in slow motion at four times the normal speed, all images were re-named based on real-world time. Calculations were then performed for the XYZ-axis distribution of particle diffusion based on each frame's image.

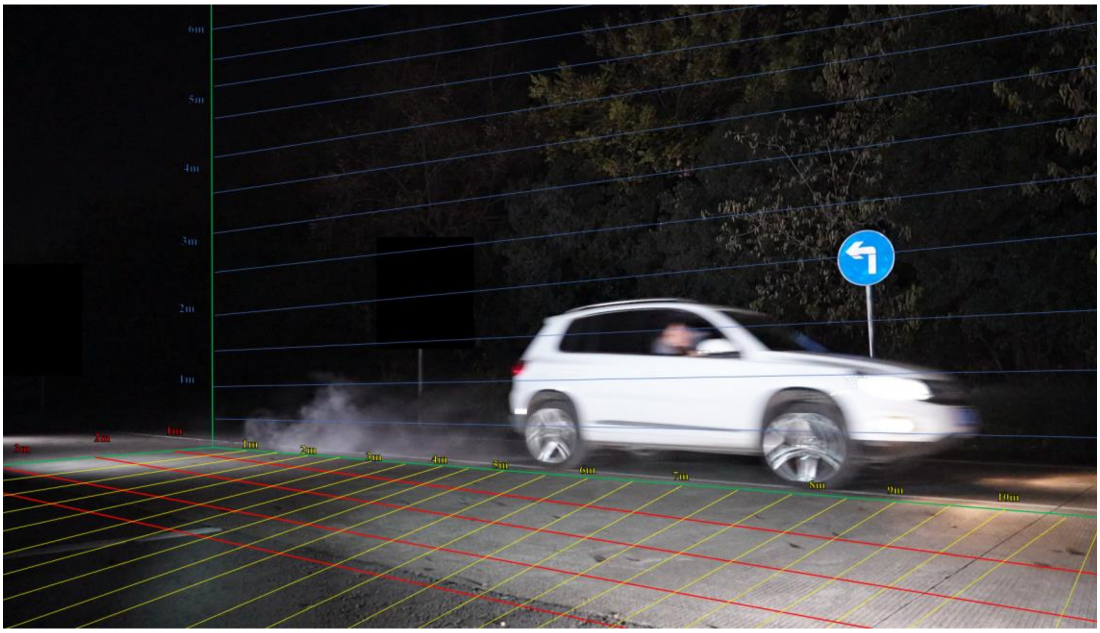

(a)

(b)

Figure 5. Capture the shot from the video with three-dimensional coordinate: (a) Camera 1 (b) Camera 2

3.3 The experiment method of "Road PM monitoring"

3.3.1 Monitoring equipment and modifications

The previous experiment analyzed particle diffusion using visual images, while this experiment validates the findings by measuring actual road particulate matter (PM) concentrations. The particle counter model used is the Temtop PMS10, manufactured by Elitech Technology, Inc., United States. To monitor PM concentrations both vertically and horizontally on the road, modifications to the particle counters are necessary. For vertical monitoring, the particle counters are placed in a fixture basket equipped with a power source and a carbon fiber rod marked with length indicators. For both horizontal and vertical monitoring, a 2.5-meter rod is used, with particle counters placed at various layers along the rod, as shown in Figure 6.

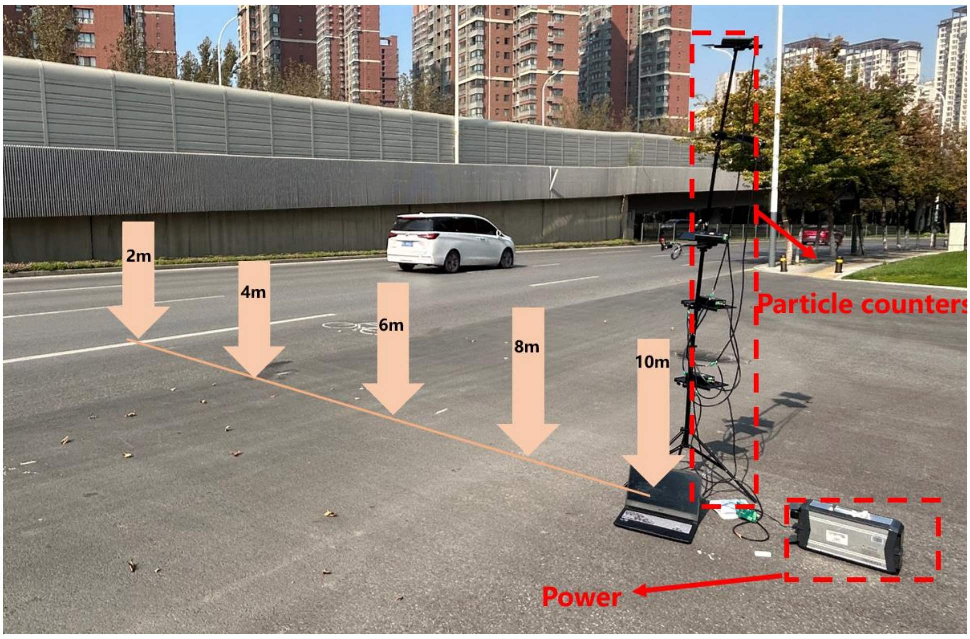

Figure 6. Monitoring sites at lateral and vertical of the road

3.3.2 Lateral and vertical diffusion patterns detection

The modified particle counter is suspended for monitoring on the road, with the counter oriented toward the direction of oncoming traffic. The selected test site is the middle segment of the South Third Ring Road in Xi'an, Shaanxi Province, China. The experiment involves positioning six particle counters on racks at various heights. The monitoring devices are placed at distances of 2 m, 4 m, 6 m, 8 m, and 10 m from the wheel track belt, with each point monitored for approximately 10 minutes, as shown in Figure 6.

3.3.3 Driving direction diffusion patterns detection

For monitoring PM concentration in the driving direction, a particle counter is placed 2 m laterally from the wheel track and at a height of 1.5 m. The selected monitoring location is Baiyun Avenue in Baiyun District, Guangzhou. Unlike the previous experiment, Baiyun Avenue, though an urban expressway, is controlled by traffic signals. Consequently, traffic flow is intermittent, as illustrated in Figure 7 (a) and (b). Continuous monitoring at this location is conducted for two hours, with data recorded every 6 seconds.

(a) (b)

Figure 7. Monitoring sites at driving direction of the road

4. Results and discussion

4.1 LPLM induced by vehicle

The experiment took place on November 30, 2023, in Xi'an, Shaanxi Province. The experimental period was from 19:00 to 22:00. The environment temperature was 13 degrees Celsius; the relative humidity was 44%, and the wind speed was 0.2 m/s.

4.1.1 Residue material analysis

4.1.1.1 Different spreading amount

First, the approximate pattern of particle resuspension and diffusion can be deduced from the video process: as the vehicle's wheels approach the particles, the air between the tire and the ground is compressed. This increased air pressure causes the particles to overcome inertia and become suspended. As the wheels pass over the particles, a vacuum negative pressure zone is created between the wheels and the ground, causing the particles to be resuspended again and subsequently affected by the wake. From the binary and pseudo-colored images of residual particles (as shown in Figure 8), it can be observed that particles with different spreading amounts exhibit the same diffusion pattern at the same vehicle speed. This is likely due to the consistent air compression between the tire and the ground when the tire rolls at a constant speed, resulting in uniform air pressure. Similarly, after the tire passes, the vacuum suction force behind the tire remains consistent. The pseudo-colored images reveal that, regardless of the spreading amount, areas with thicker residual particles correspond to the tread's indentations due to the texture compressing against the ground. All pseudo-colored images indicate no significant differences in the quantity of residual particles.

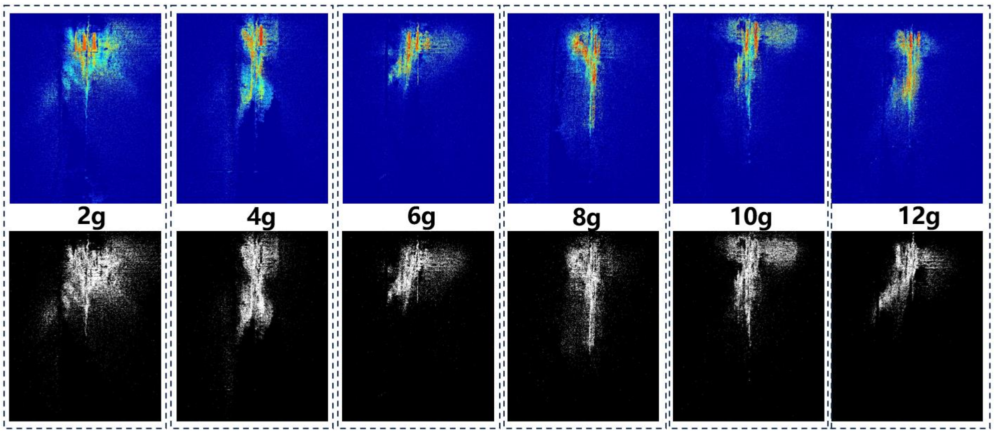

Figure 8. Pseudo-colored images of residual particles of different spreading mount

4.1.1.2 Different vehicle speed

Figure 9 illustrates the residual particles on the ground after traveling at different vehicle speeds, with a spreading amount of 10 g per square decimeter. The graph clearly shows that as vehicle speed increases, the area covered by the residual particles decreases, and the diffusion distance shortens. This is because, at lower speeds, the air pressure between the tire and the ground is relatively lower when the tires are about to crush the particles. As a result, the particles do not become suspended but instead spread on the ground and disperse around after being crushed by the wheels. In contrast, vehicles traveling at higher speeds generate sufficient air pressure and suction between the tires and the ground, allowing particles to disperse more effectively into the air.

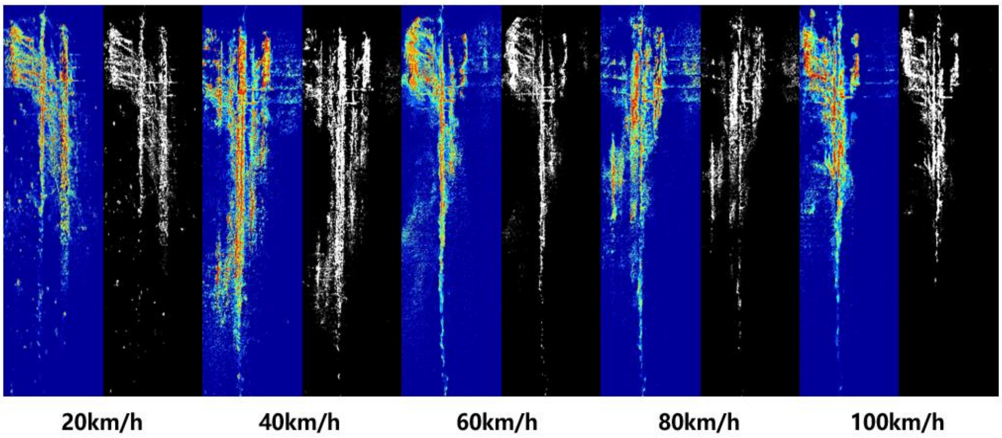

Figure 9. Pseudo-colored images of residual particles of different vehicle speed

4.1.2 The diffusion patterns of re-suspended particles

4.1.2.1 Spreading amount

Establishing the relationship between particle diffusion distance along the XYZ-axis and time, this experiment selects the visible edge of particle diffusion (the farthest one) as the calculated distance due to the non-uniformity of all diffusion particles. Figure 10 illustrates the relationship between the diffusion distance of particles along the X-axis and time. From the video frames shown in Figure 10, it can be observed that particle diffusion along the X-axis can be divided into three stages:

(1) Stage I (Compression Dominated Zone): When the tire is about to make contact with the ground, the air in the region between them is compressed, causing particles on the ground to be entrained and lifted, rapidly diffusing along the X-axis. This stage occurs almost instantaneously, lasting approximately 0.25 seconds, with a particle diffusion speed of 10 m/s.

(2) Stage II (Wake Dominated Zone): After the particles are crushed by the front and rear wheels, they begin to diffuse along the X-axis under the influence of the vehicle's wake. This diffusion occurs at a slower rate than in Stage I, lasting about 1 second, with a particle diffusion speed ranging from 3.5 m/s to 6.4 m/s.

(3) Stage III (Turbulent Flow Dominated Zone): As the particles gradually detach from the vortex and due to the vacuum created by the vehicle's passage, a negative pressure zone forms behind the vehicle. Air drawn into this zone slowly induces particle diffusion along the X-axis, with a particle diffusion speed ranging from 2.4 m/s to 2.8 m/s, as shown in Figure 11(a).

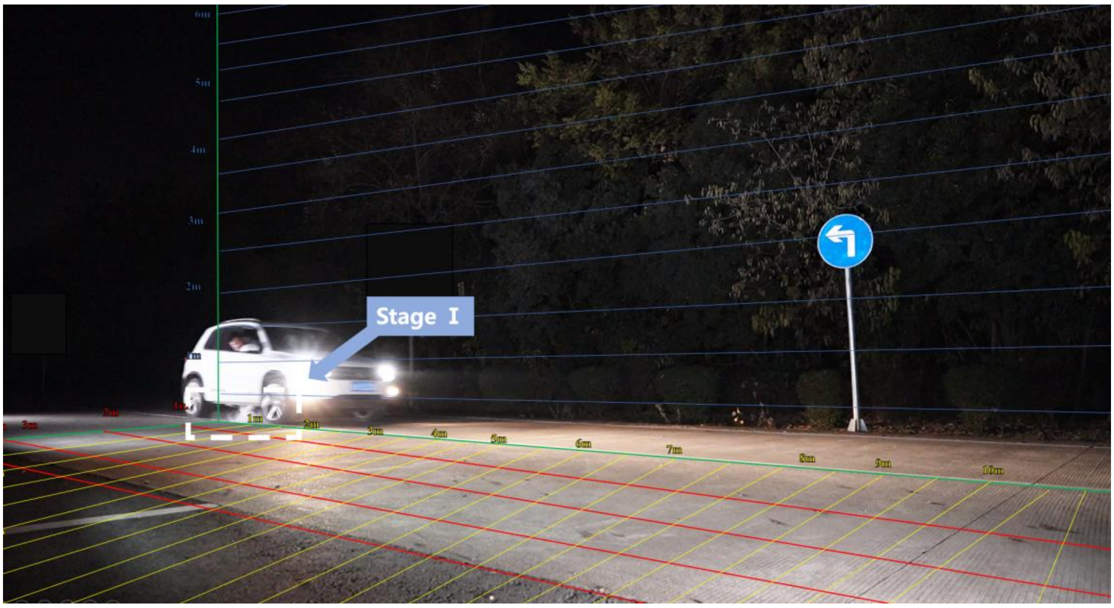

(a)

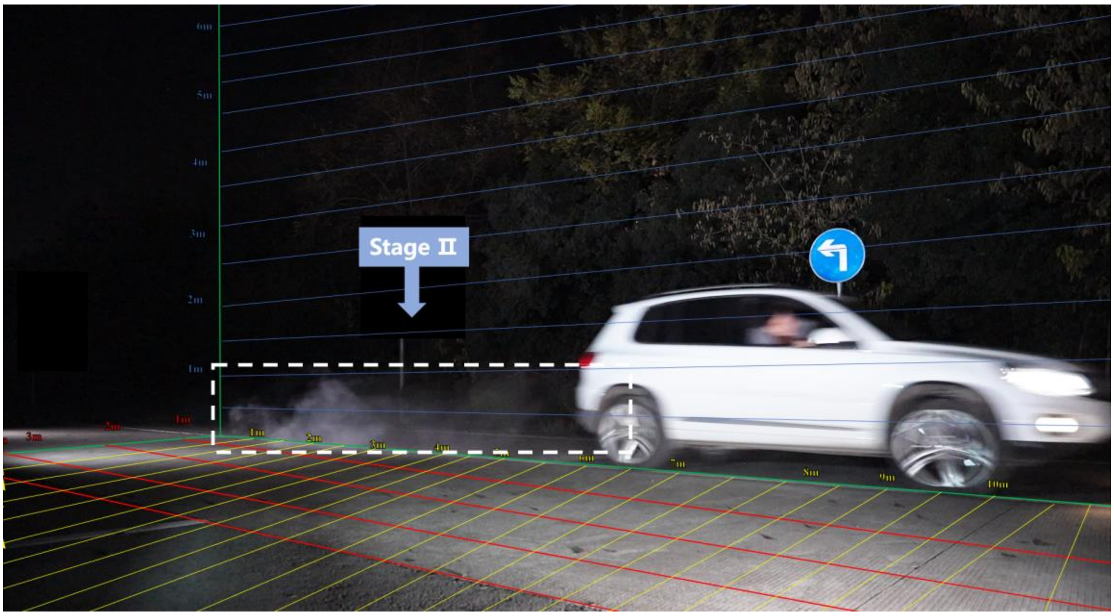

(b)

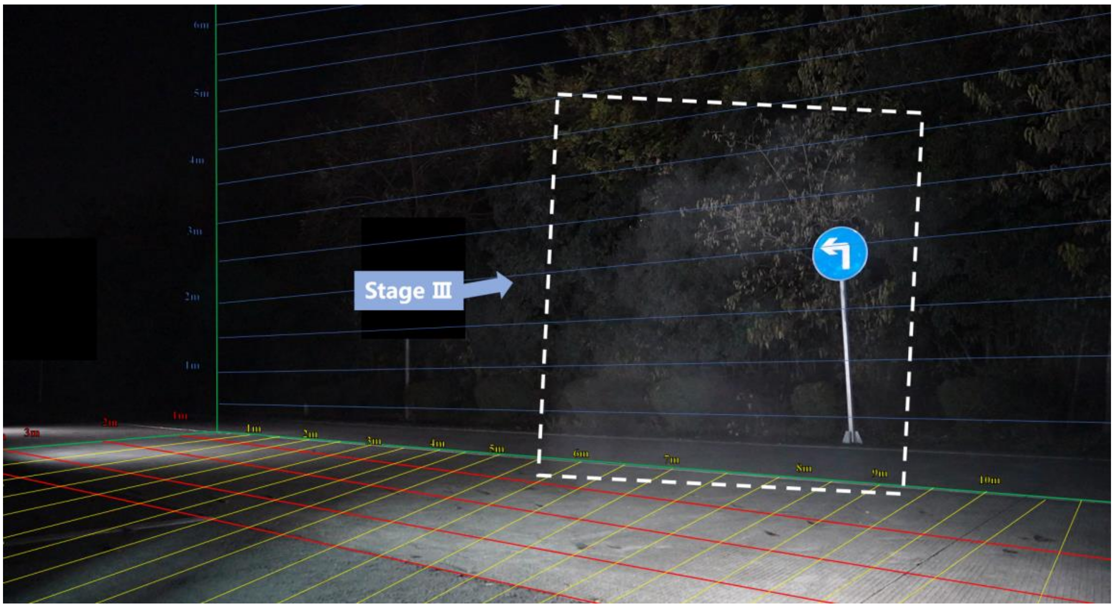

(c)

Figure 10. Particle diffusion pattern in X-axis: (a) Stage I (b) Stage II (c) Stage III

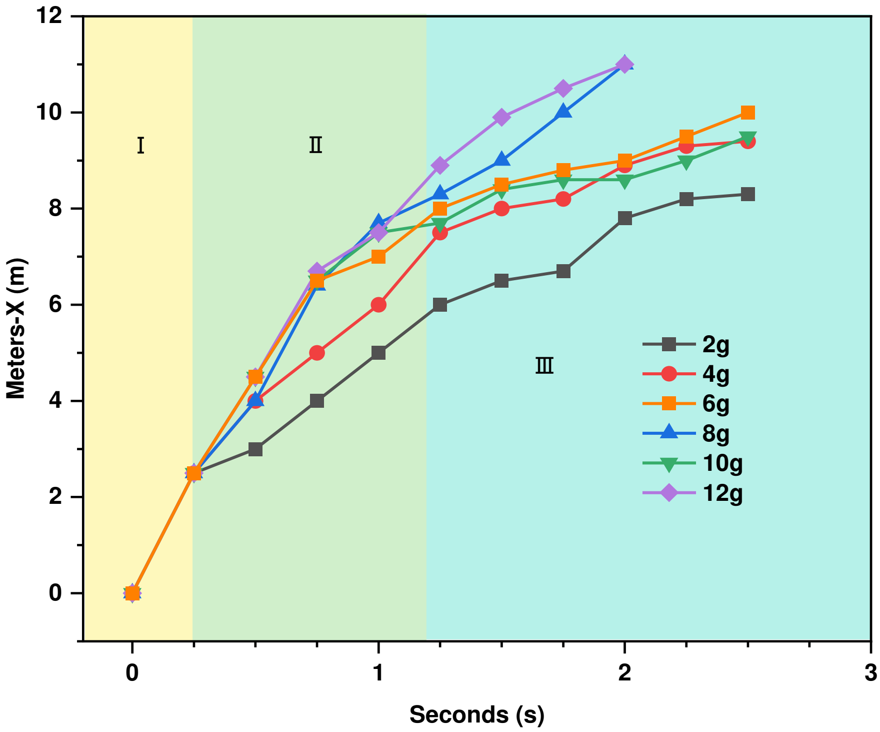

12
10
8
6
4
2
0
Meters-X (m)
0
1
2
3
Seconds (s)
Ⅰ
Ⅱ
Ⅲ
2g
4g
6g
8g
10g
12g

(a)

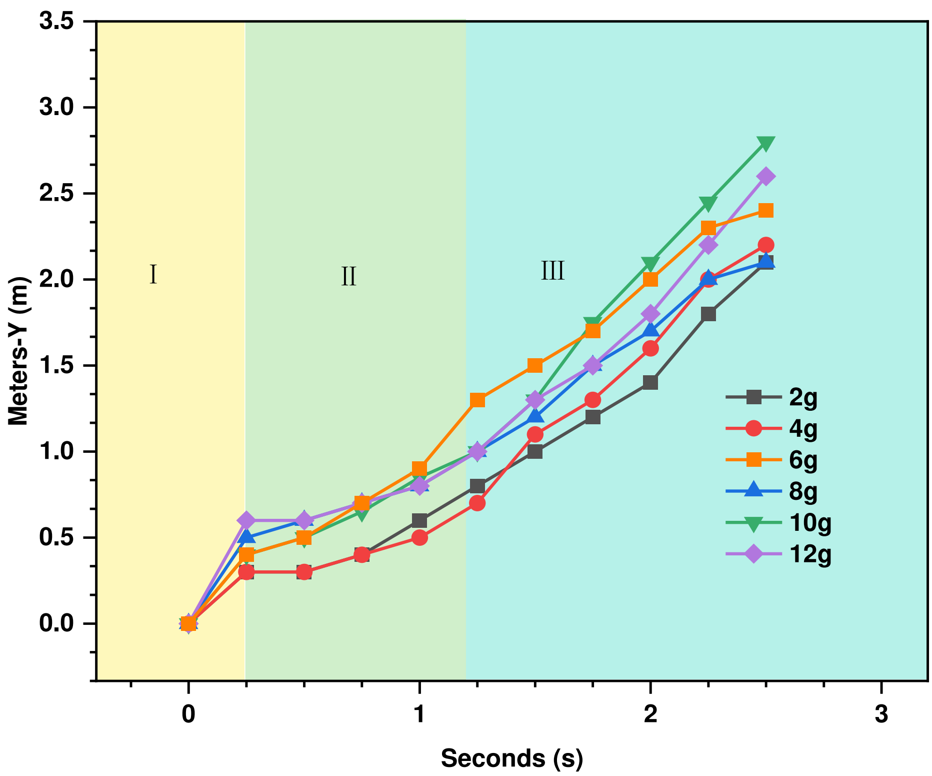

3.5
3.0
2.5
2.0
1.5
1.0
0.5
0.0
Meters-Y (m)
0
1
2
3
Seconds (s)
I
II
III
2g
4g
6g
8g
10g
12g

(b)

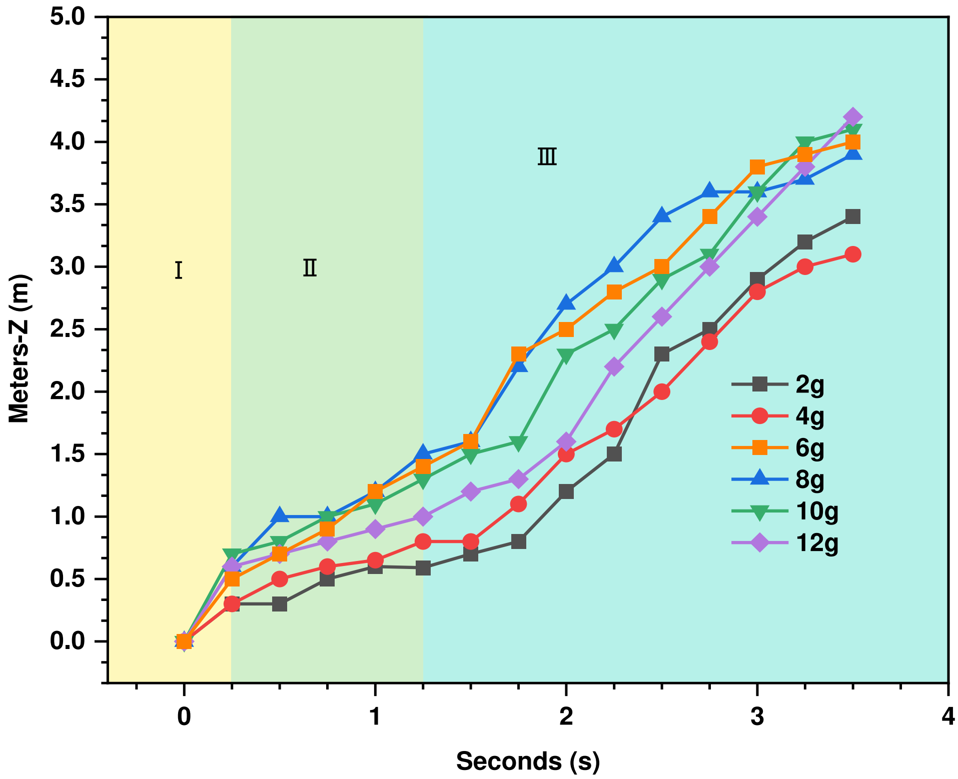

(c)

Figure 11. The relationship of time-diffusion distance of X, Y, Z-axis: (a) X (b)Y (c) Z

The relationship between diffusion distance along the Y and Z axes and time is illustrated in Figures 11(b) and 11(c). This relationship can be divided into three stages, similar to the X-axis. In Stage I, as the tire is about to crush the particles, they rapidly diffuse in the Y and Z directions. In Stage II, the vehicle's wake causes more diffusion along the X-axis rather than in the Y and Z directions, which differs from the diffusion pattern observed along the X-axis. In Stage III, as particles detach from the wake, the influx of air leads to significant diffusion along the Y and Z axes. Overall, the diffusion rate along the Y and Z axes is higher in Stage I, slows down in Stage II, and increases again in Stage III.

4.1.2.2 Vehicle speed

There are significant differences in particle diffusion depending on vehicle speed and the amount of material spread. Figure 12 illustrates the relationship between diffusion distance along the XYZ-axis and time at various vehicle speeds. The graph shows that diffusion along the X-axis can be divided into three stages, but the duration of these stages varies with vehicle speed. For instance, at 100 km/h, the Stage I lasts approximately 0.25 seconds, during which the outermost contour of the particles can reach 4 meters. As vehicle speed decreases, this value gradually reduces. Additionally, vehicle speed affects the distance that the wake drags the particles along the X-axis. At speeds of 100 km/h, 80 km/h, 60 km/h, 40 km/h, and 20 km/h, the second stage's X-axis distances are 7.0 m, 6.7 m, 6.2 m, 5.5 m, and 3.0 m, respectively. Thus, as speed increases, the time spent in Stages I and II decreases, resulting in longer overall diffusion distances. Conversely, at slower speeds, the diffusion distance in Stages I and II is less and lasts longer. This variation is likely due to differences in the velocity of the wake generated by vehicles traveling at different speeds. Figure 12 highlights the time and length of Stages I and II at 100 km/h, with transition points between Stages I, II, and III at other speeds indicated by dashed boxes.

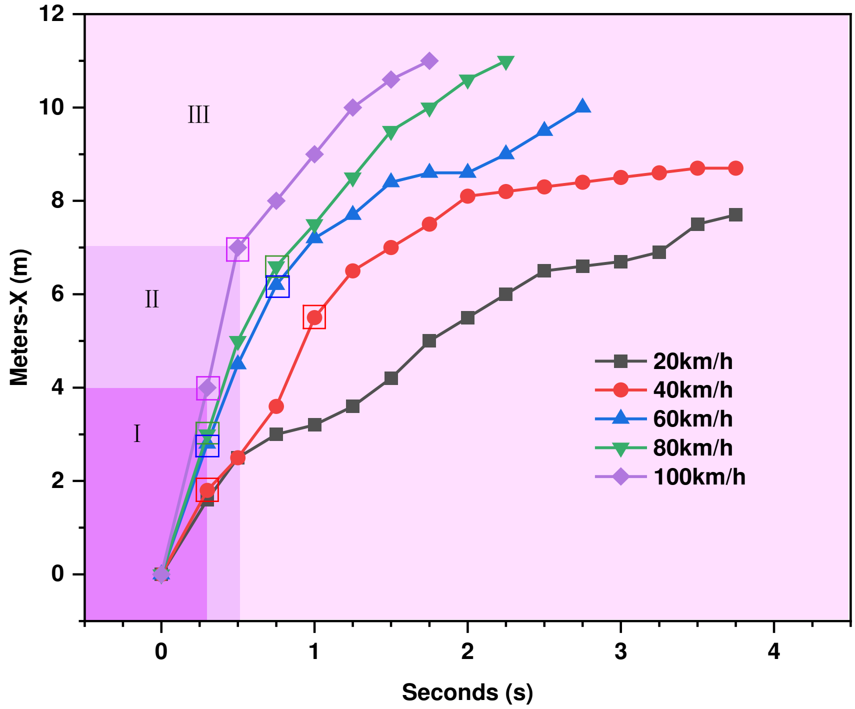

12
10
8
6
4
2
0
Meters-X (m)
III
II
I
20km/h
40km/h
60km/h
80km/h
100km/h
0
1
2
3
4
Seconds (s)

(a)

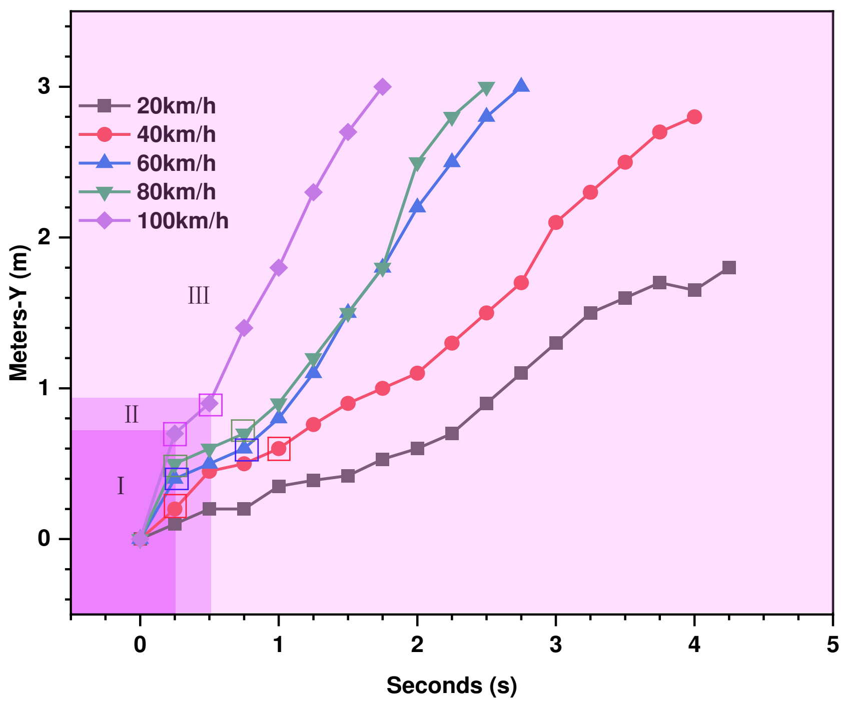

3
2
1
0
Meters-Y (m)
20km/h
40km/h
60km/h
80km/h
100km/h
III
II
I
0
1
2
3
4
5
Seconds (s)

(b)

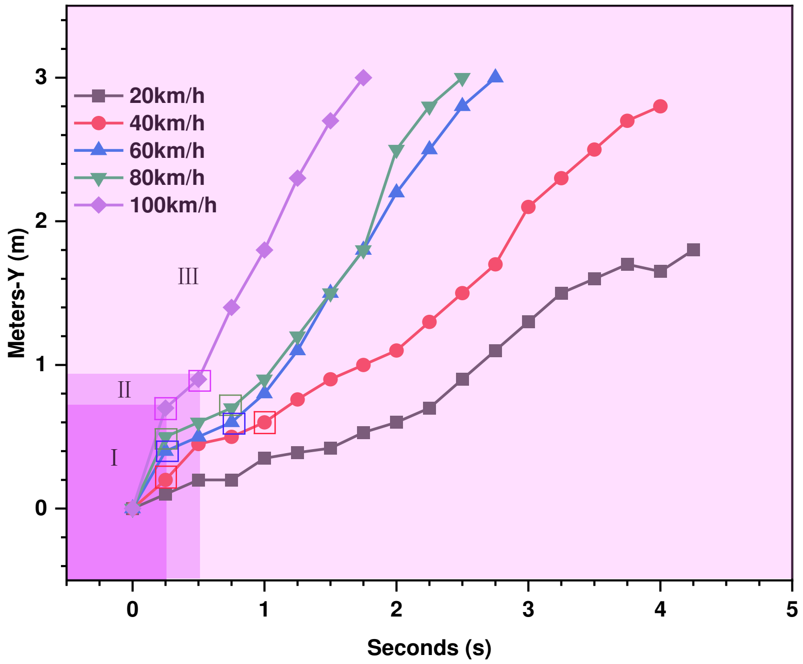

(c)

Figure 12. The relationship between the diffusion distance of XYZ-axis and time at different vehicle speeds: (a) X (b) Y (c) Z

The relationship between the diffusion distance along the Y and Z axes and time under different vehicle speeds is consistent across varying scattering amounts, as shown in Figures 12 (b) and (c). However, the duration and distance covered in each of the three stages vary with speed. Generally, the faster the speed, the shorter the duration and distance of Stage II. At lower speeds (20 km/h or 40 km/h), there is little difference between Stages I and II. When calculating the maximum suspension height of particles at different speeds, it is observed that higher speeds result in greater suspension heights. The relationship between maximum suspension height and velocity closely follows a quadratic polynomial fit, with an R^2 value of 0.997, as shown in Figure 13.

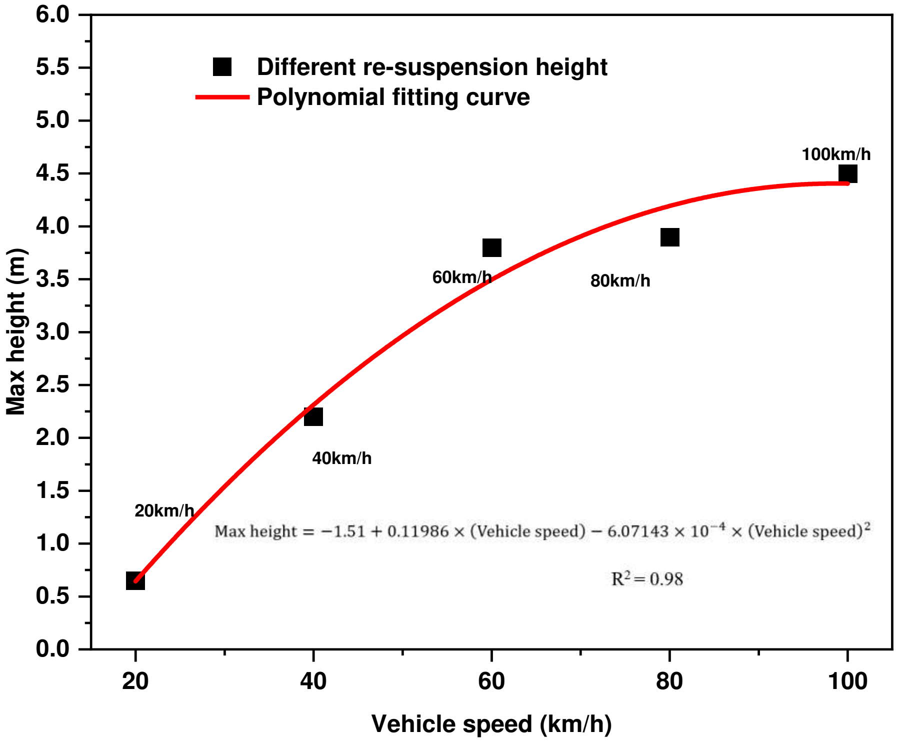

Figure 13. The relationship between max diffusion height at different speed

To calculate the diffusion area of particles in the XYZ axis, the outermost contour of the particles is depicted, as shown in the Figure 14 (a). For a more intuitive understanding of the lateral, longitudinal, and vertical distribution of particles, project the three-dimensional contour lines onto the XOY, YOZ, and XOZ planes, as Figure 14 (b) shows.

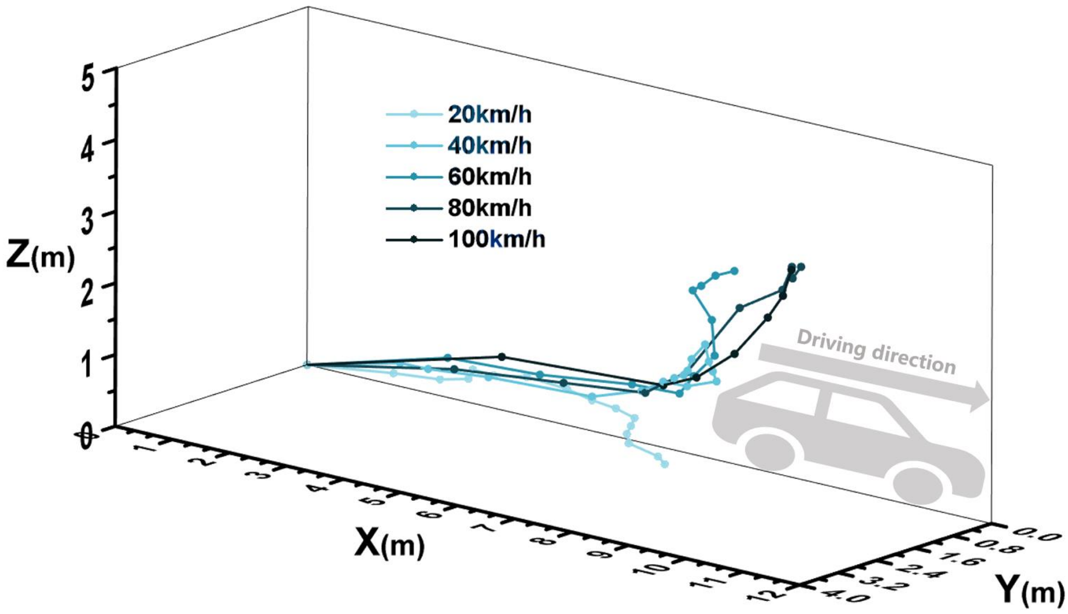

(a)

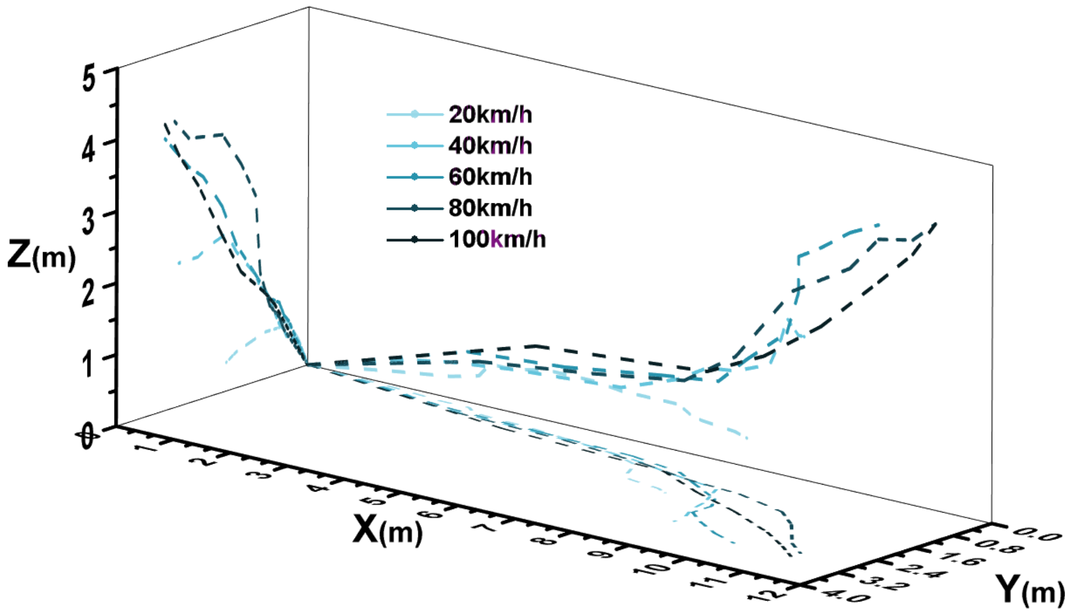

(b)

Figure 14. The 3D contour lines of diffusion particles and their mapping

The Figure 15 (a), (b) and (c) are maps of the outer contour lines. The relationship between the diffusion area and time shows three stages, and the contour lines also exhibit the same pattern. From the YOZ diagram, it can be observed that the general trend is that the faster the vehicle speed, the higher the diffusion of particles. From the XOY plane, it is evident that with increasing vehicle speed, particles diffuse over a greater distance. Lastly, from the XOZ perspective, it can be seen that higher vehicle speeds lead to particles diffusing over a greater distance. Therefore, overall, higher vehicle speeds tend to result in larger areas of particle diffusion outward.

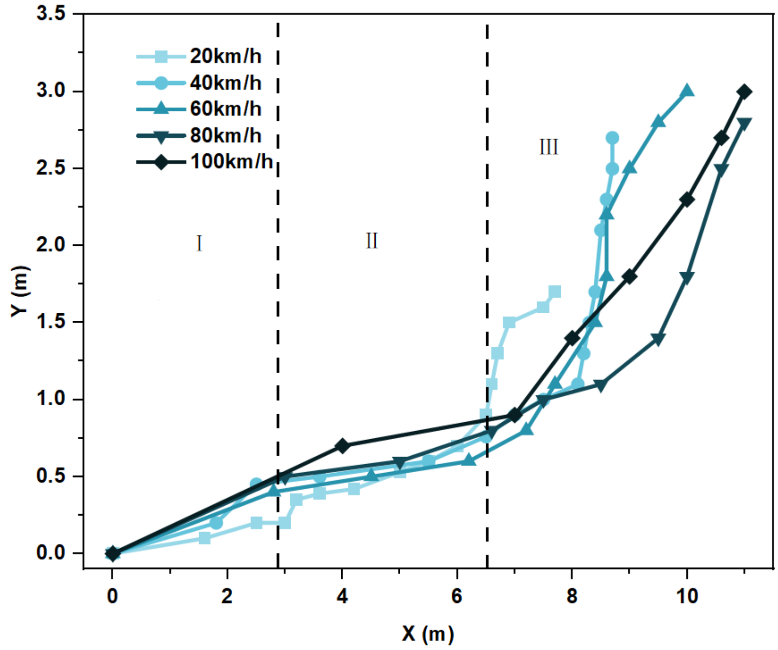

(a)

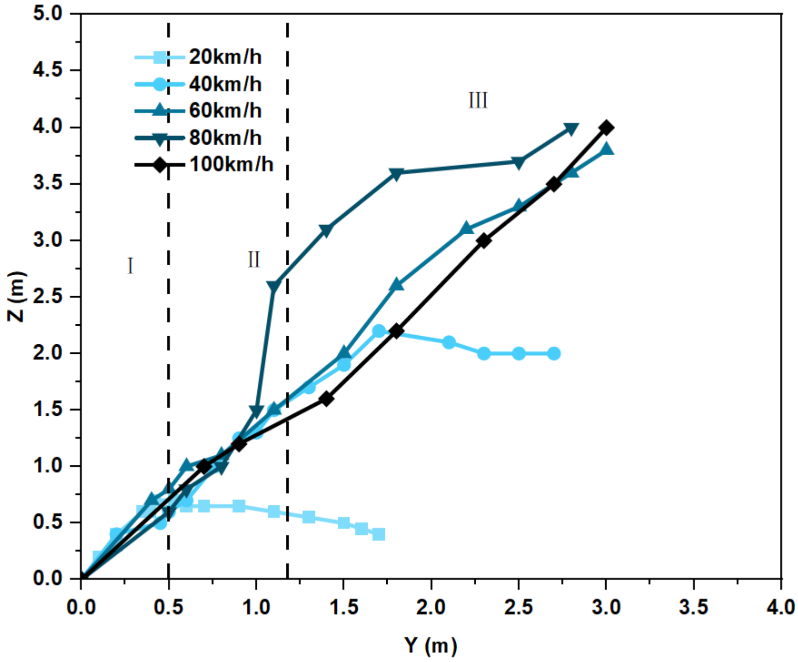

(b)

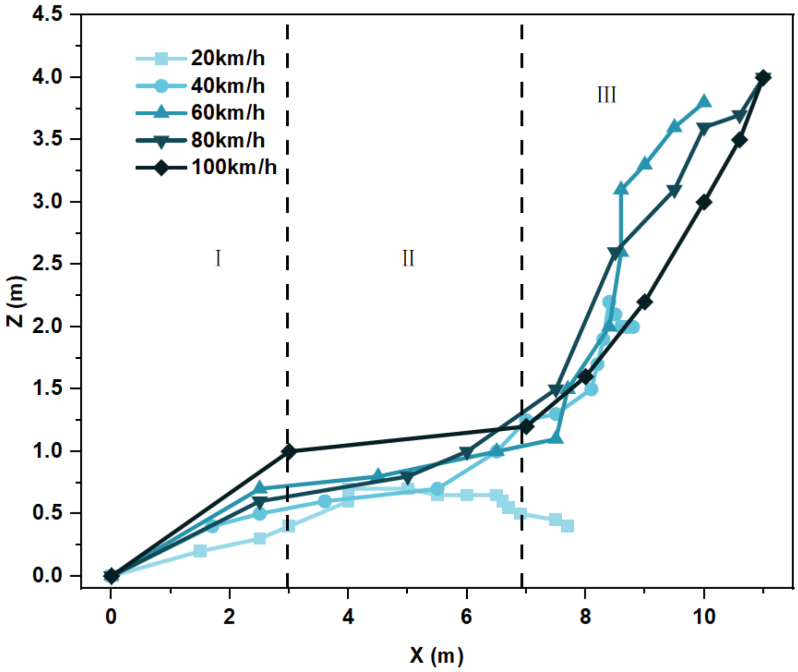

(c)

Figure 15. The maps of the outer contour lines: (a)YOZ-axis (b)XOY-axis (C)XOZ-axis

4.2 Road PM monitoring

4.2.1 Lateral and vertical diffusion patterns

The following figures present data from dust monitors positioned at 2 m, 4 m, 6 m, 8 m, and 10 m distances from the roadside after modification. Figure 16 (a) shows measurements taken during the morning rush hour with an average road speed of 20 km/h, while Figure 16 (b) depicts measurements taken at midday with an average road speed of 40 km/h. In Figure 16 (a), it can be observed that the area with the highest PM_{10} concentration is at 2 m laterally, followed by 4 m, 6 m, 8 m, and 10 m respectively. When the vehicle speed is relatively high (40 km/h), there is a change in the diffusion pattern, with the maximum concentration shifting to 4 m laterally, followed by 2 m, 6 m, 8 m, and 10 m, as Figure 16 (b) shows.

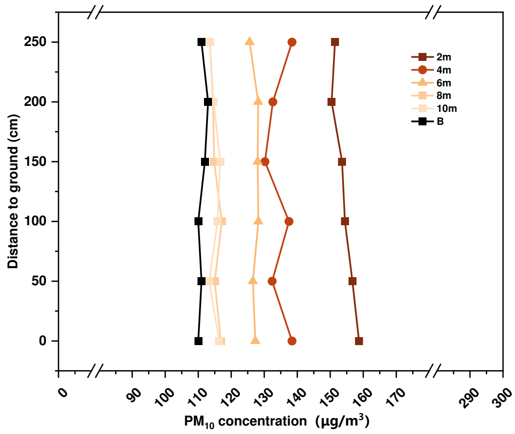

(a)

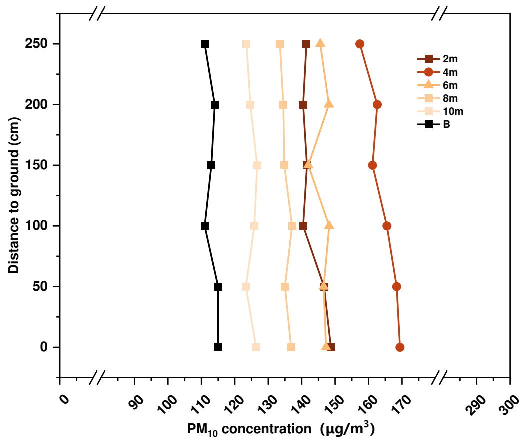

(b)

Figure 16. The results of PM monitoring: (a) 20km/h (b) 40km/h

The Figure 17 displays lateral diffusion area contour maps based on LPLM experiments. The red area represents the particle diffusion area within 2 m from the track, while the blue area represents the diffusion area between 2 m and 4 m. It can be observed that when the vehicle speed is 40 km/h, nearly half of the area (top left corner) within 2 m laterally has no particles, while particles at 2 m to 4 m laterally have not yet settled completely. This explains why the PM_{10} concentration at 4m laterally is higher than at 2 m when the vehicle speed is higher. However, when the vehicle speed is slower, particles within 2 m have completed suspension-settling, thus resulting in a higher PM_{10} concentration at 2 m than at 4 m.

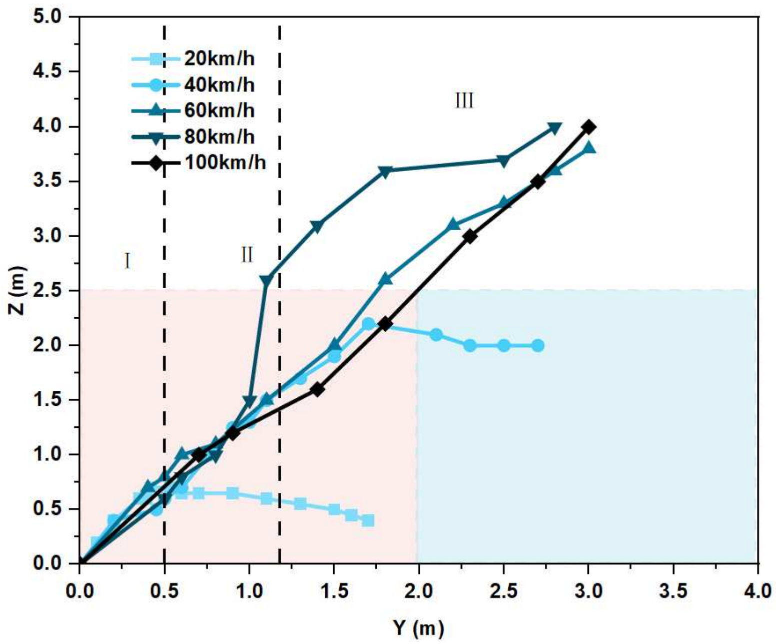

Figure 17. Lateral diffusion area contour maps

4.2.2 Driving direction diffusion patterns

Figure 18(a) presents monitoring data collected over a two-hour period. The data shows that PM_{10} concentrations exhibit periodic fluctuations, characterized by a continuous and smooth transition from low to high levels and back again. Figure 18(b) highlights a smaller segment of this data, indicating that it takes approximately three minutes for the PM_{10} concentration to rise from its lowest to its highest point, followed by a similar descent. Comparing this with on-site traffic flow conditions, it was observed that PM_{10} concentrations begin to decrease as traffic moves past the monitor and start to rise again after the traffic has passed. This suggests that particulate matter does not disperse immediately as vehicles pass by but instead begins to spread to the surroundings after a brief delay.

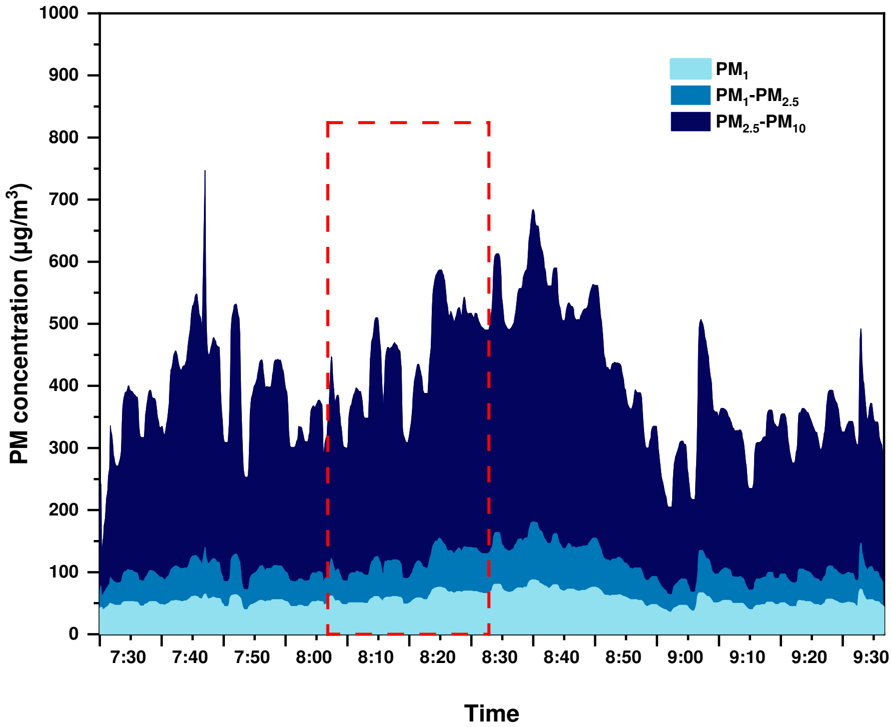

(a)

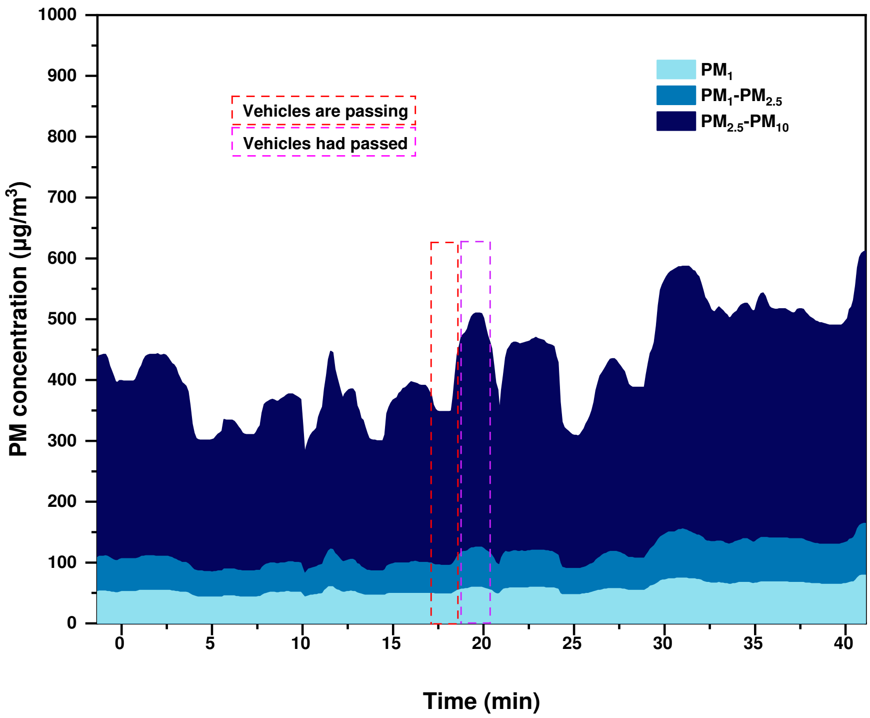

(b)

Figure 18. The results of driving direction diffusion patterns

5. Discussion

The resuspension mechanism of particulate matter can be roughly divided into three parts from a visual perspective. The first part involves tire-road contact, where the interaction between the tire and the road surface causes the particulate matter to overcome inertia and detach from the ground. This process includes the compression of air between the tire's front wall and the ground, the significant suction behind the tire to the ground, and the detachment of particulate matter as it adheres to and rotates with the tire. The second part is the wake region, where the wake carries the particulate matter forward in the direction of travel. These particles primarily disperse within a small area and exhibit minimal lateral or vertical diffusion. Finally, in the turbulence stage, the low-pressure zone generated at the rear of the vehicle as it moves draws in surrounding air, leading to the lateral and vertical diffusion of the particulate matter due to the turbulence.

The maximum diffusion distance that particles can reach under different spreading amounts and vehicle speeds was statistically analyzed, as shown in Figure 19. It is observed that, regardless of the spreading amount and vehicle speed, both the spreading amount and vehicle speed significantly influence the distance particles disperse, with greater spreading amounts and higher vehicle speeds resulting in farther particle diffusion. This pattern is consistent across all X, Y, and Z axes. The effect of vehicle speed on diffusion distance is notably greater than that of the spreading amount. Under traffic conditions, particles travel the furthest along the X-axis, followed by the Z and Y axes. The maximum diffusion distances of particles along the XYZ-axis under different vehicle speeds are as follows: 20 km/h (7.7 m, 1.8 m, 0.7 m); 40 km/h (8.7 m, 3.0 m, 2.2 m); 60 km/h (11.0 m, 3.0 m, 3.8 m); 80 km/h (11.0 m, 3.0 m, 4.0 m); and 100 km/h (11.0 m, 3.0 m, 4.5 m).

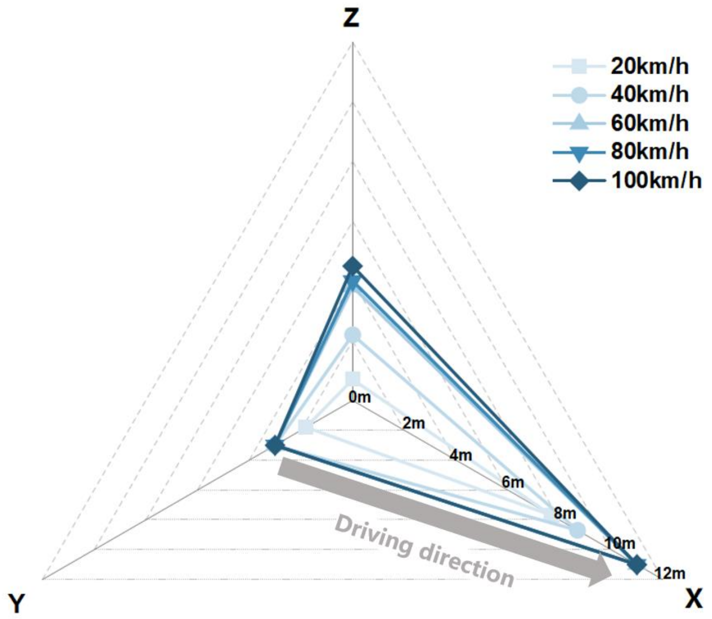

(a)

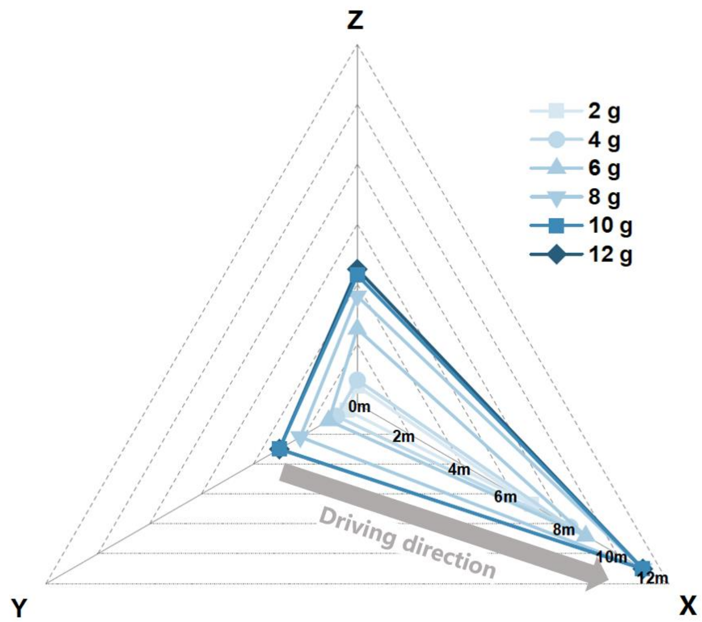

(b)

Figure 19. The maximum diffusion distance: (a) different vehicle speeds (b) different spreading amounts

Experimental observations reveal that as vehicle speed increases, the force exerted by the tire compressing air against the ground and the vacuum suction effect behind the tire both intensify, along with the wake effect, causing particles to disperse farther. In experiments with different spreading amounts at the same vehicle speed, it was found that when the spreading amount is small, most particles tend to adhere to the tire and do not become airborne. However, as the spreading amount increases, more particles become suspended, resulting in a greater diffusion distance with higher spreading amounts. The maximum diffusion distances of particles along the XYZ-axis under different spreading amounts are as follows: 2 g (6.7 m, 0.4 m, 0.6 m); 4 g (8.2 m, 0.8 m, 0.8 m); 6 g (8.8 m, 1.1 m, 2.5 m); 8 g (11.0 m, 2.2 m, 3.6 m); 10 g (11.0 m, 3.0 m, 4.3 m) and 12 g (11.0 m, 3.0 m, 4.5 m).

The experimental site was chosen as a closed and clean cement road to ensure data accuracy. This choice was necessitated by the fact that outdoor asphalt concrete surfaces are heavily worn, complicating the differentiation between originally deposited dust and long-persistence phosphor material. In previous studies, some researchers have found that road surfaces with large voids are not conducive to the resuspension of dust. Therefore, to enable the dust to be maximally suspended in the air and investigate its patterns. Thus, the use of a cement road surface eliminates the potential interference from voids within asphalt concrete, which might trap particles and prevent their resuspension. Due to the wide-angle coverage of the camera, the study's observational area was restricted to 11 m × 6 m × 3 m, which proved inadequate. Data indicate that at vehicle speeds exceeding 60 km/h, the particle diffusion area extends beyond the boundaries of the camera's field of view. While relocating the camera to a greater distance could capture a broader frame, it would also result in blurred particle contours.

Future studies should employ higher-definition equipment to enhance observational precision.

Direct imaging of the fluorescence emitted by long-persistence phosphors was not feasible with the camera. Consequently, the Tyndall effect was employed to augment visibility through additional light sources. Nighttime filming was utilized to maximize the intrinsic luminosity of the particles and create a stark contrast between the reflected light and the background. Preliminary experiments (not discussed in this paper) indicated that optimal results were obtained with the camera positioned perpendicular to the lane. However, for this study, which required capturing diffusion patterns in all XYZ directions, an oblique angle of 45° was used.

In calculating particle diffusion distances, the "outermost point"—the farthest dispersed area of the particles—was used as the reference. Due to the small size of the particles, the camera could only capture particle aggregation at specific moments. Once disturbed by turbulence, the particles disperse in multiple directions, resulting in incomplete recording and data loss as particles descend along the XYZ-axis. Observations of residual particles reveal that, after compression by the tires, they tend to accumulate in the texture grooves on the surface.

6. Conclusion

This paper simulates the behavior of re-suspended road dust using long persistence luminescence materials and specific vehicles on clean enclosed sections of cement concrete roads. It calculates the diffusion patterns of re-suspended particles over time, and it computes the maximum width, height and distance of dust diffusion along the direction of vehicle movement. Finally, the study is validated through on-road experiments. The conclusions are as follows:

1. The suction between the tread and the ground is the most significant influencing condition for the re-suspension of particulate matter deposited on the ground after being rolled over. Analysis of particulate matter deposited on the ground indicates that particles tend to remain trapped in grooves. Consequently, tire tread patterns with larger enclosed areas are more likely to cause dust resuspension.
2. The wake generated after a vehicle passes carries the re-suspended particles forward in the direction of its formation without causing lateral or vertical diffusion. The greater the vehicle speed, the longer the travel distance. In areas where traffic slows down or stops, such as pedestrian crosswalks, the lateral and vertical diffusion of dust becomes more pronounced. These areas are also densely populated by pedestrians, making it essential to enhance measures for mitigating resuspended dust.
3. After particles detach from the wake, the negative pressure behind the vehicle causes the suspended particles to diffuse laterally and vertically. The greater the amount of particulate matter deposited on the ground and the higher the vehicle speed, the greater the diffusion height and width are. Therefore, for the design of high-grade urban roads with higher vehicle speeds, the spacing between the sidewalk and the roadway should be appropriately increased.

4. Pedestrians on overpasses and cyclists should be protected from the health hazards posed by particles due to their vertical diffusion. The faster the vehicle speed, the greater the lateral diffusion distance. Therefore, sidewalks and cycle paths should be positioned at a certain distance from the roadway during the planning and provision of infrastructure for active travel.
5. The maximum diffusion distances of particles along the XYZ axes under different vehicle speeds are as follows: 20 km/h (7.7 m, 1.8 m, 0.7 m); 40 km/h (8.7 m, 3.0 m, 2.2 m); 60 km/h (11.0 m, 3.0 m, 3.8 m); 80 km/h (11.0 m, 3.0 m, 4.0 m); and 100 km/h (11.0 m, 3.0 m, 4.5 m). The maximum diffusion distances of particles along the XYZ axes under different spreading amounts are as follows: 2 g (6.7 m, 0.4 m, 0.6 m); 4 g (8.2 m, 0.8 m, 0.8 m); 6 g (8.8 m, 1.1 m, 2.5 m); 8 g (11.0 m, 2.2 m, 3.6 m); 10 g (11.0 m, 3.0 m, 4.3 m) and 12 g (11.0 m, 3.0 m, 4.5 m). Their relationship between maximum height and vehicle speed approximates a polyno mial curve, with an R^2 of 0.98.

7. Recommendations

Future research will focus on studying the resuspension patterns of fine particulate matter (less than 10 μm) across different vehicle types, tire tread patterns, and road surface types. Additionally, this study aims to provide data for mitigating road dust re-suspension and for computational fluid dynamics simulations (CFD).

Conflicts of Interest

No competing financial interests exist.

Funding

This work was supported by the National Natural Science Foundation of China (Grant No.52311530081 and 52122809). Also, this work was supported by Key R&D Projects in Shaanxi Province (2024SF-YBXM-577, 2024SF-YBXM-606), the "Scientists & Engineers" Team Construction Based on Qin Chuang Yuan Platform, Shaanxi Province (2024QCY-KXJ-020).

References

Abu Khatita, A.M., 2024. Risk assessment of potentially toxic elements in street dust from Mahd Ad Dhahab gold mine, Saudi Arabia. *Journal of Taibah University for Science* 18(1).

Alves, C.A., Vicente, A.M.P., Calvo, A.I., Baumgardner, D., Amato, F., Querol, X., Pio, C., Gustafsson, M., 2020. Physical and chemical properties of non-exhaust particles generated from wear between pavements and tyres. *Atmospheric Environment* 224, 117252.

Budai, P., Clement, A., 2018. Spatial distribution patterns of four traffic-emitted heavy metals in urban road dust and the resuspension of brake-emitted particles: Findings of a field study. *Transportation Research Part D: Transport and Environment* 62, 179-185.

Casotti Rienda, I., Nunes, T., Gonçalves, C., Vicente, A., Amato, F., Lucarelli, F., Kovάts, N., Hubai, K., Sainnokhoi, T.-A., Alves, C.A., 2023. Road dust resuspension in a coastal Atlantic intermunicipal urban area with industrial facilities: Emission factors, chemical composition and ecotoxicity. *Atmospheric Research* 294, 106977.

Chae, E., Jung, U., Choi, S.-S., 2024. Types and concentrations of tire wear particles (TWPs) in road dust generated in slow lanes. *Environmental Pollution* 346, 123670.

Chen, W., Wang, Y., Zeng, W., Han, S., Li, G., Guo, H., Li, Y., Qiang, Q., 2016. Long persistent composite phosphor CaAl2O4:Eu2+,Nd3+/Y3Al5O12:Ce3+: a novel strategy to tune the colors of persistent luminescence. *New Journal of Chemistry* 40(1), 485-491.

Dan, H.-C., Lu, B., Li, M., 2024. Evaluation of asphalt pavement texture using multiview stereo reconstruction based on deep learning. *Construction and Building Materials* 412, 134837.

Deng, Z., Jin, W., Yin, Q., Huang, J., Huang, Z., Fu, H., Yuan, Y., Zou, J., Nie, J., Zhang, Y., 2021. Ultrasensitive visual detection of Hg(2+) ions via the Tyndall effect of gold nanoparticles. *Chem Commun (Camb)* 57(21), 2613-2616.

Edwards, L., Wilkinson, P., Rutter, G., Milojevic, A., 2022. Health effects in people relocating between environments of differing ambient air pollution concentrations: A literature review. *Environmental Pollution* 292, 118314.

Grange, S.K., Fischer, A., Zellweger, C., Alastuey, A., Querol, X., Jaffrezo, J.-L., Weber, S., Uzu, G., Hueglin, C., 2021. Switzerland's PM10 and PM2.5 environmental increments show the importance of non-exhaust emissions. *Atmospheric Environment: X* 12, 100145.

Guerreiro, C., Ortiz, A.G., Leeuw, F.D., Viana, M., Horάlek, J., 2016. *Air quality in Europe — 2016 report.* Air quality in Europe — 2016 report.

He, C., Jiang, W., 2024. Research on particle size distribution and composition of road deposit dust in Xi'an: From the perspective of non-exhaust emissions. *Journal of Cleaner Production* 470, 143269.

He, C., Jiang, W., Wang, T., Yuan, D., Sha, A., 2024. The evolution of tire-road wear particles and road surface texture under rolling friction. *Construction and Building Materials* 447, 138167.

Huang, J.K., Mo, X.M., Fu, H.Y., Sun, Y., Gao, Q., Chen, X.J., Zou, J.M., Yuan, Y.L., Nie, J.F., Zhang, Y., 2021. Tyndall-effect-enhanced supersensitive naked-eye determination of mercury (II) ions with silver nanoparticles. *Sensors and Actuators B-Chemical* 344.

Jandacka, D., Durcanska, D., Cibula, R., 2022. Concentration and inorganic elemental analysis of particulate matter in a road tunnel environment (Zilina, Slovakia): Contribution of non-exhaust sources. *Frontiers in Environmental Science* 10.

Jeong, C.H., Wang, J.M., Hilker, N., Debosz, J., Sofowote, U., Su, Y.S., Noble, M., Healy, R.M., Munoz, T., Dabek-Zlotorzynska, E., Celo, V., White, L., Audette, C., Herod, D., Evans, G.J., 2019. Temporal and spatial variability of traffic-related PM2.5 sources: Comparison of exhaust and non-exhaust emissions. *ATMOSPHERIC ENVIRONMENT* 198, 55-69.

Jiang, R., Liu, Y., Hu, D., Zhu, L., 2022. Exhaust and non-exhaust airborne particles from diesel and electric buses in Xi'an: A comparative analysis. *Chemosphere* 306, 135523.

Jiang, W., Wang, T., Yuan, D., Sha, A., Zhang, S., Zhang, Y., Xiao, J., Xing, C., 2024. Available solar resources and photovoltaic system planning strategy for highway. *Renewable and Sustainable Energy Reviews* 203, 114765.

Laniyan, T.A., Popoola, O.J., 2024. Integrated Assessment of Heavy Metal Contamination in Urban Road Dust: Implications for Human Health and Ecosystem Sustainability in Abeokuta, Nigeria. *Environmental Forensics*.

Li, J., Cui, D., Yang, Z., Ma, J., Liu, J., Yu, Y., Huang, X., Xiang, P., 2024. Health risk assessment of heavy metal(loid)s in road dust via dermal exposure pathway from a low latitude plateau provincial capital city: The importance of toxicological verification. *Environmental Research* 252, 118890.

Li, Y., Gecevicius, M., Qiu, J.R., 2016. Long persistent phosphors-from fundamentals to applications. *Chemical Society Reviews* 45(8), 2090-2136.

Liu, J.J., Wang, J.Y.W., Liu, Y., Wang, L.L., Long, L.L., He, J.S., Huang, C.Y., Shen, F., Zhang, Y.Z., 2024. A hygroscopic dual-porous road dust suppressant with good dust suppression prepared by the freeze-thawing method. *Journal of Cleaner Production* 448.

Liu, Y., Jin, T., Yu, S.H., Chu, H.Q., 2023. Pollution characteristics and health risks of heavy metals in road dust in Ma'anshan, China. *Environmental Science and Pollution Research* 30(15), 43726-43739.

Roy, A., Mandal, M., Das, S., Kumar, M., Popek, R., Awasthi, A., Giri, B.S., Mondal, K.C., Sarkar, A., 2024. Non-exhaust particulate pollution in Asian countries: A comprehensive review of sources, composition, and health effects. *Environmental Engineering Research* 29(3).

Samiksha, S., Sunder Raman, R., Nirmalkar, J., Kumar, S., Sirvaiya, R., 2017. PM(10) and PM(2.5) chemical source profiles with optical attenuation and health risk indicators of paved and unpaved road dust in Bhopal, India. *Environ Pollut* 222, 477-485.

Shan, J., Jiang, W., Huang, Y., Yuan, D., Liu, Y., 2024. Unmanned Aerial Vehicle (UAV)-Based Pavement Image Stitching Without Occlusion, Crack Semantic Segmentation, and Quantification. *IEEE Transactions on Intelligent Transportation Systems*, 1-16.

Svensson, N., Lundberg, J., Janhäll, S., Kulovuori, S., Gustafsson, M., 2023. Effects of a porous asphalt pavement on dust suspension and PM10 concentration. *Transportation Research Part D: Transport and Environment* 123, 103921.

Timmers, V., Achten, P.A.J., 2016. Non-exhaust PM emissions from electric vehicles. *ATMOSPHERIC ENVIRONMENT* 134, 10-17.

Van den Eeckhout, K., Poelman, D., Smet, P.F., 2013. Persistent Luminescence in Non-Eu²⁺-Doped Compounds: A Review. *Materials* 6(7), 2789-2818.

Verma, S., Kumar, D., Dutta, S., Sharma, V., Swart, H.C., Kumar, V., 2020. A novel near white light emitting phosphor KSrYSi2O7:Dy3+: Synthesis, characterization and luminescence properties. *Vacuum* 174.

Wagner, S., Funk, C.W., Müller, K., Raithel, D.J., 2024. The chemical composition and sources of road dust, and of tire and road wear particles – A review. *Science of The Total Environment* 926, 171694.

Wang, J., Du, C., Chen, Z., Wang, Y., 2023. Influence of vehicle and pavement characteristics on dust resuspension from soil pavement of open-pit mine. *Science of The Total Environment* 878, 163252.

Wang, L., Wu, Y., Wang, Y., Yu, L., Song, G., 2024. Modeling Urban-Rural health disparities using a Taxi-Based mobile atmospheric monitoring system. *Transportation Research Part D: Transport and Environment* 129, 104152.

Wang, Y., Huang, Z.H., Liu, Y.J., Yu, Q., Ma, W.C., 2017. Back-Calculation of Traffic-Related PM10 Emission Factors Based on Roadside Concentration Measurements. *ATMOSPHERE* 8(6).

Wu, W., Jiang, W., Xiao, J., Yuan, D., Wang, T., Ling, X., 2024a. Investigation of LAS-based fatigue evaluation methods for high-viscosity modified asphalt binders with high-content polymers. *Construction and Building Materials* 422, 135810-135810.

Wu, W.J., Cavalli, M.C., Jiang, W., Kringos, N., 2024b. Differing perspectives on the use of high-content SBS polymer-modified bitumen. *Construction and Building Materials* 411.

Xiao, W.C., Deng, Z.H., Huang, J.K., Huang, Z.H., Zhuang, M.M., Yuan, Y.L., Nie, J.F., Zhang, Y., 2019. Highly Sensitive Colorimetric Detection of a Variety of Analytes via the Tyndall Effect. *Analytical Chemistry* 91(23), 15114-15122.

Yang, Y., Su, X., Xu, Y., Jin, W., Shen, B., Zhang, X., Lv, R., He, Y., Guo, C., Li, Y., Zou, J., 2023. Study on the Relationship Between Tea Concentration and Tyndall effect. *E3S Web Conf. (France)*, 03018 (03017 pp.)-03018 (03017 pp.).

Yu, C., Deng, Y., Qin, Z., Yang, C., Yuan, Q., 2023. Traffic volume and road network structure: Revealing transportation-related factors on PM2.5 concentrations. *Transportation Research Part D: Transport and Environment* 124, 103935.

Zou, F., Leng, Z., Li, D., Zhang, S., Yaphary, Y.L., Lu, G., 2023. Leaching potential of metals and PAHs of asphalt rubber paving materials. *Transportation Research Part D: Transport and Environment* 125, 103984.